Capillary transfer of soft films

Yue Zhang[a,1], Mengtian Yin[a,1], Yongmin Baek[b], Kyusang Lee[b], Giovanni Zangari[c], Liheng Cai[c], and Baoxing Xu[a,2]

[a]Department of Mechanical and Aerospace Engineering, University of Virginia, Charlottesville, VA 22904; [b]Department of Electrical and Computer Engineering, University of Virginia, Charlottesville, VA 22904; and [c]Department of Materials Science and Engineering, University of Virginia, Charlottesville, VA 22904

Edited by John A. Rogers, Northwestern University, Evanston, IL, and approved January 27, 2020 (received for review January 10, 2020)

Existing transfer technologies in the construction of film-based electronics and devices are deeply established in the framework of native solid substrates. Here, we report a capillary approach that enables a fast, robust, and reliable transfer of soft films from liquid in a defect-free manner. This capillary transfer is underpinned by the transfer front of dynamic contact among receiver substrate, liquid, and film, and can be well controlled by a selectable motion direction of receiver substrates at a high speed. We demonstrate in extensive experiments, together with theoretical models and computational analysis, the robust capabilities of the capillary transfer using a versatile set of soft films with a broad material diversity of both film and liquid, surface-wetting properties, and complex geometric patterns of soft films onto various solid substrates in a deterministic manner.

flexible structures | capillary transfer | soft films | liquid substrate

Films with a low flexural rigidity, referred hereto as "soft" films that could be made of a wide variety of materials, not only intrinsically soft materials with a low modulus such as elastomeric/polymeric materials of polydimethylsiloxane (PDMS), but also stiff/brittle materials with micro/nanoscale thickness such as ultrathin silicon membrane (1) and metal foils (2), are the basis for an entire class of wearable technologies in flexible electronics/optoelectronics (3, 4), biomedical devices (5, 6), energy storage and conversion systems (7–9), and micro/nanoelectromechanical systems (10, 11). Unfortunately, existing technologies that enable a mechanical transfer of these soft films onto receiver substrates for practical applications are based on their as-fabricated, growth or intermediate solid substrates such as glass slides, semiconductor wafers, and native metals. Besides, these processes usually require assistance of external stimuli such as heating (12) or/and chemical etching (13) with sophisticated structural designs and fabrications that help reduce the interfacial energy and facilitate the physical separation of films, and rely largely on trial-and-error methods, which results often in a low yield and inevitable contamination, degradation, and/or damage to films (14, 15). Compared with solid native substrates, the liquid phase, an intrinsically deformation-free substrate due to fluidity, provides a unique and tactful platform that helps release residual stress or/and avoid deformation mismatch with surrounding solid constraints during growth, self-assembly, and fabrication of materials and structures, and is emerging as a powerful host medium in the preparation of a wide variety of functional films from 2D materials (16), to Janus films (17), and to biofilms (18). Moreover, the fluidity of liquid would allow films to move upwards or downside the liquid substrate, which enabled a selective contact of the two film surfaces with the receiver substrates. However, the conventional transfer approaches and fundamentals of films that are deeply established in the framework of native solid substrates are not applicable for developing a scalable, fast, and defect-free transfer technology toward a reliable transferring of film from liquid surface.

Here, we report a capillary approach that enables a fast transfer of soft films from a versatile set of noncorrosive liquid environment in a defect-free manner. This capillary transfer is underpinned by a transfer front that is a dynamic interface of contact among solid receiver substrate, liquid native substrate, and transfer film with a small capillary force, and can be well controlled by moving the direction (push down or pull up) of receiver substrates in a high speed, thereby leading to a damage- and defect-free film delivery with a desirable surface in contact with the receiver substrate. We demonstrate in extensive experiments, together with theoretical models and computational analysis, the capillary transfer of a versatile set of soft films with a broad material diversity of both film and liquid, thickness, surface-wetting properties, and geometric patterns of soft films onto various solid substrates in a well-defined order. With a combination of the push-down and pull-up transfers, we further demonstrate the application capability of capillary transfer in the assembly of multiple-layer structures with a desirable assembly order. Our approach offers a scalable route for transferring soft films of complex patterns and on-demand surface functions onto substrates, potentially useful for fabrication, assembly, and patterning of film-based devices, structures, and systems.

Results

Mechanics and Mechanism of Capillary Transfer. The working principle of this capillary transfer technology is illustrated in Fig. 1*A*, where one end of the receiver substrate is submerged in the liquid bath to form the initial contact line among substrate, soft film, and liquid, referred to as the transfer front (orange dotted line "P"). Upon the motion of the substrate in an either pull-up or push-down direction, the film will detach from the liquid surface and gradually transits onto the substrate across the transfer front that remains unchanged, until the entire film is transferred onto the substrate. After the transfer, with the pull-up direction, the bottom surface of film (in blue) will be in contact with the substrate and the top surface (in red) is exposed to air; by contrast,

Significance

Soft films are the basis for an entire class of wearable technologies in flexible electronics and biomedical devices. The capillary transfer approach reported here establishes a rational route for the fast transfer of soft films from liquid onto a solid substrate in a well-defined order that allows achieving deterministic assembly of structures with complex layouts and patterns for applications in the fabrication of flexible electronics, surface wetting structures, and optical devices. The developed theoretical models along with validations from extensive experiments and computational analysis provide a fundamental understanding of solid-liquid interactions in response to external mechanical stimuli that can be leveraged in the exploration of emerging fabrication and self-assembly technologies with a broad scope of materials and liquid environments.

Author contributions: B.X. designed research; Y.Z., M.Y., Y.B., K.L., and B.X. performed research; Y.Z. and M.Y. contributed new reagents/analytic tools; Y.Z., M.Y., and B.X. analyzed data; and Y.Z., M.Y., G.Z., L.C., and B.X. wrote the paper.

The authors declare no competing interest.

This article is a PNAS Direct Submission.

[1]Y.Z. and M.Y. contributed equally to this work.

[2]To whom correspondence may be addressed. Email: bx4c@virginia.edu.

This article contains supporting information online at https://www.pnas.org/lookup/suppl/doi:10.1073/pnas.2000340117/-/DCSupplemental.

First published February 24, 2020.

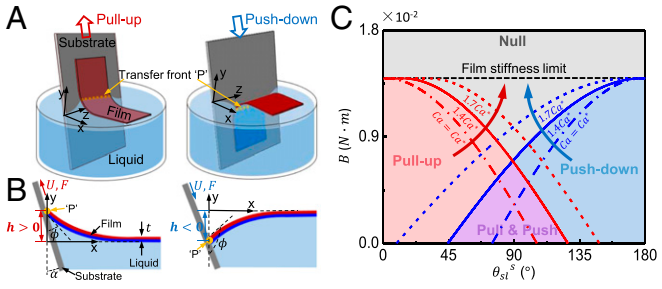

Fig. 1. Illustration of the capillary transfer technology and its capillary-elastic analysis in theory. (*A*) Schematic illustration of the capillary transfer. Upon the motion of the receiver substrate in an either pull-up or push-down direction (α) under a force F at a velocity U, the film (thickness t, colored to distinguish the top and bottom side) will detach from the liquid surface and gradually transit across the contact line among substrate, soft film and liquid (referred to as the transfer front, orange dotted line P) to the substrate, until the entire film is transferred onto the substrate. The location of transfer front P remains unchanged during the transfer process. After a successful transfer, with the pull-up transfer, the bottom surface of film (in blue) in initial contact with liquid will be in contact with the substrate and the top surface (in red) is exposed to air; by contrast, with the push-down transfer, the top surface of film will be in contact with the substrate and the bottom surface of film is exposed to air. (*B*) Schematic illustration (cross-section view) of the theoretical model for the capillary-elastic analysis at the transfer front P. At the transfer front, the film will be bent by the capillary force and the consequent ϕ and h is the tangential direction of the bent film at the transfer front and the height of the transfer front P, respectively. For the pull-up transfer, the film needs to be bent upward ($h>0$) by the capillary force; for the push-down transfer, the film needs to be bent downward ($h<0$). $h=0$ suggests the capillary force is small enough and cannot bend the film, and the film cannot be transferred to the substrate, which corresponds to its maximum bending stiffness. (*C*) Theoretical phase diagram on the choice of the transfer direction with respect to materials (bending stiffness of soft film B, the static contact angle of substrate to the liquid θ_{sl}^s) and loading conditions (capillary number Ca that depends on substrate moving velocity), where $Ca^* = 6 \times 10^{-5}$ (for pull-up direction), 2×10^{-4} (for push down direction). The blue and red area suggests conditions for the push-down and pull-up direction, respectively, the purple area is the condition where both directions are feasible, and the gray area is the condition where the film cannot be transferred. The black dotted line corresponds to the limit of maximum bending stiffness of film.

with the push-down direction, the top surface will be in contact with the substrate and the bottom surface of the film is exposed to air. At the initial state of transfer with the substrate moving velocity U, the soft film will be mechanically bent at the transfer front by the capillary force (Fig. 1*B*), and the bending deformation depends on the bending stiffness of the film, wettability of substrate and film to liquid, and transfer velocity U. With a negligible elongation and local deformation of the soft film at the transfer front (see Theoretical Analysis in *Materials and Methods*), the geometric profile of the bent soft film is $y = he^{-x\sqrt{\rho g/\gamma_l}}$, where γ_l and ρ are the surface tension and density of liquid, respectively. $h = \sqrt{\frac{\gamma_l}{\rho g}}\cot\phi$ is the height of the transfer front relative to the liquid surface and ϕ represents the tangential direction of the bent film at the transfer front with respect to the vertical ($-y$) direction. The pull-up transfer requires that the transfer front must be above the liquid surface to allow the film to pass by moving upwards, and we have $h>0$ associated with the bending upwards of the film (i.e., $\phi<90^o$); by contrast, the push-down transfer requires the transfer front to be below the liquid surface to allow the film to pass by moving downward, and we have $h<0$ associated with bending downward of the film (i.e., $\phi>90^o$). $h=0$ suggests that the capillary force is too small to bend the film ($\phi=90^o$), and the film cannot be transferred to the substrate, which corresponds to the limit of flexural rigidity. The essential deformation of the film reflects the energy balance between elastic bending deformation ($E_{bending}$) and solid–liquid interaction ($E_{surface}$) and can be quantified through the total energy $E_t = E_{bending} + E_{surface}$, where $E_{bending} = \int \frac{1}{2}\left(\frac{Bb_t}{12}\right)(y''/(1+y'^2)^{3/2})^2(1+y'^2)^{1/2}dx$, $E_{surface} = -\gamma_l\cos\theta_{sl}^d b_t\frac{h}{\cos\alpha}$, where $B = Et^3$ is the bending stiffness of film, E, t, and b_t are the elastic modulus, thickness, and width of film, respectively; γ_l is the surface tension of liquid, α is the direction of substrate relative to the vertical ($-y$) direction, and θ_{sl}^d is the dynamic contact angle of substrate to the liquid. Further, define the advancing and receding contact angle of substrate to liquid θ_{sl}^a, and θ_{sl}^r, respectively, and the moving velocity of substrate relative to liquid U, when the substrate is pushed down into the liquid, we will have $\theta_{sl}^d = \theta_{sl}^a$, and the rate dependence of θ_{sl}^a is described by the equation $(\theta_{sl}^a)^3 - (\theta_{sl}^s)^3 = k_\varepsilon \cdot Ca$ (19), where $Ca = \frac{\mu U}{\gamma_l}$ is the capillary number, μ is the liquid viscosity, and θ_{sl}^s is the static contact angle of substrate to liquid. k_ε depends on the slip length and for example $k_\varepsilon = 3.2\times10^4$ for liquid water and PDMS substrate (*SI Appendix*, Figs. S1 and S2*B*). Similarly, when the substrate is pulled up out of the liquid, we will have $\theta_{sl}^d = \theta_{sl}^r$, and $(\theta_{sl}^s)^3 - (\theta_{sl}^r)^3 = k_\varepsilon \cdot Ca$, where $k_\varepsilon = 2.8\times10^3$ for liquid water and glass substrate (*SI Appendix*, Figs. S1 and S2*C*). The minimization of total energy E_t will be utilized to determine h that helps predict the transfer direction by adjusting the properties of soft film, liquid environment, and transfer substrate (Fig. 1*C*). Besides, a large α will lead to a small minimum total energy E_t with an increased magnitude of the height h (*SI Appendix*, Fig. S3 *A* and *B*) and is beneficial for achieving a successful transfer by both pull-up and push-down transfers. *SI Appendix*, Fig. S3*C* summarizes the effect of these transfer conditions on the selection of transfer directions. These theoretical phase diagrams show that a more hydrophobic transfer substrate and a higher capillary number Ca will be beneficial for the push-down transfer. By contrast, a more hydrophilic transfer substrate will be beneficial for the pull-up transfer.

As an example, the glass with a hydrophilic surface and PDMS with a hydrophobic surface were chosen as model transfer substrates to demonstrate the pull-up and push-down transfer of a PDMS soft film (slightly dyed for visualization) with thickness t about 200 μm from a liquid water bath at the speed of 0.1 mm/s, respectively. At the beginning, the magnitude of transfer force for both push-down and pull-up transfers shows an increase with the increase of displacement (Fig. 2*A*). Once the film transfer initiates, it decreases until the onset of a steady-state stage with a constant magnitude. At the end of transfer, the force gradually recovers back to that of initial transfer. Compared with their corresponding transfer force–displacement curves without film transfer, the drop of the transfer force for both transfer directions at the steady-state stages is observed and reflects the effect of film on the interaction between substrate and liquid. Upon completion, successful transfers of PDMS films onto both the glass and PDMS substrates via pull-up and push-down transfers, respectively, are obtained (Fig. 2*B* and Movies S1 and S2). More importantly, with the pull-up transfer, the bottom surface of PDMS film in initial contact with water (labeled in B) adheres to the substrate and the top surface (labeled in T) is exposed to air; with the push-down transfer, the bottom surface of film is exposed to air instead. Similar results are obtained in the transfer for different film materials, thicknesses, and moving velocities (*SI Appendix*, Fig. S4 *A* and *B*), which are in good agreement with theoretical predictions in Fig. 1*C*. We further predict the transfer force F_s at the steady-state process (see Theoretical Analysis in *Materials and Methods*). At $Ca < 0.01$, where the effect of viscosity can be neglected (*SI Appendix*, Fig. S5), they are simplified to $F_s = 2b_s\gamma_l\cos(((\theta_{sl}^s)^3 - k_\varepsilon\cdot Ca)^{1/3}) + b_t(-G_{ts} + \gamma_l\cos\theta_{tl} + \gamma_l)$ for pull-up transfer and $F_s = (-2b_s\gamma_l + b_t\gamma_l)\cos(((\theta_{sl}^s)^3 + k_\varepsilon\cdot Ca)^{1/3}) + b_t(-G_{ts} + \gamma_l)$ for push-down

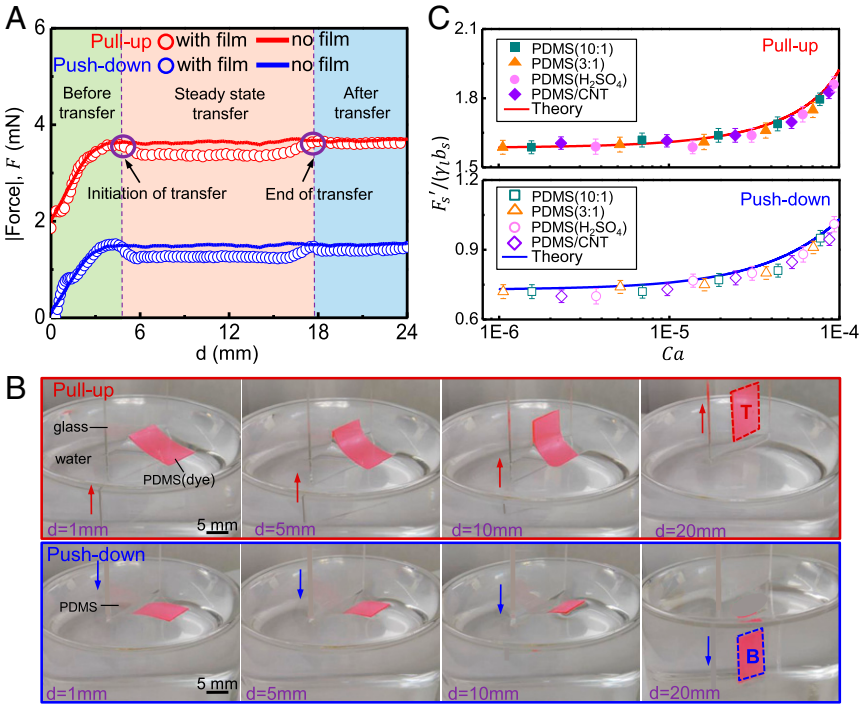

Fig. 2. Characterization of mechanics behavior during capillary transfer. (*A*) The variation of magnitude of the transfer force (F) with the moving displacement of substrate (d) during the capillary transfer process with and without film in both pull-up (in red) and push-down (in blue) directions. The direction of force is upward in pull-up transfer and downward in push-down transfer. In the pull-up and push-down experiment, the substrate is glass and PDMS slide, respectively. In both experiments, the liquid bath is water, and the film is PDMS film slightly dyed for visualization. (*B*) Optical images of the capillary transfer experiments at a series of displacements in both pull-up and push-down directions. After the pull-up transfer, the bottom surface of film in contact with water adheres to the substrate and the top surface (in red, marked with "T") is exposed to air. For the push-down transfer, the bottom surface of film in contact with water (in blue, marked with "B") is exposed to air. (*C*) Comparison of the steady-state transfer force of film normalized by the liquid surface tension (γ_l) and substrate width (b_s),$F_s'/\gamma_l b_s$, as a function of the capillary number *Ca* between the theoretical calculations and experimental measurements for a wide variety of soft-film materials in both pull-up and push-down transfers. $F_s'/\gamma_l b_s = 2\cos(((\theta_{sl}^s)^3 - k_\varepsilon \cdot Ca)^{1/3})$ for pull-up transfer, and $F_s'/\gamma_l b_s = \left(-2+\frac{b_t}{b_s}\right)\cos(((\theta_{sl}^s)^3 + k_\varepsilon \cdot Ca)^{1/3})$ for push-down transfer. The error bar represents the SD from the mean of three independent experiments.

transfer, where G_{ts} is the adhesion energy between soft film and transfer substrate and can be measured from a separate peeling test (*SI Appendix*, Fig. S6); b_s is the width of transfer substrate. These theoretical predictions of transfer force in both pull-up and push-down transfers show remarkable agreement with experimental measurements for a wide variety of film materials with different stiffness, thickness and surface wettability, transfer substrates and liquids under a series of moving velocities of transfer substrate (Fig. 2*C* and *SI Appendix*, Fig. S4). Similar to the transfer force with film, the force without the transfer of film during the pull-up and push-down processes of substrate can also be obtained and they are $F_s = 2b_s\gamma_l\cos\theta_{sl}^r$ for pull up and $F_s = -2b_s\gamma_l\cos\theta_{sl}^a$ for push down, which agrees well with experiments (Fig. 2*A*).

Design Diagrams for Pull-Up and Push-Down Capillary Transfer. Once the transfer direction of pull up or push down is determined, a successful transfer requires a continuous pass of film across the whole transfer front. The difference in the magnitude of transfer force ΔF between with and without the transfer of film at the steady state of transfer process is a straightforward and sufficient factor to formulate the criterion that guides the success of capillary transfer along both directions. For example, if $\Delta F < 0$, the pass of film across the transfer front is an energy-favorable process, and the transfer will succeed, and otherwise, the transfer will fail. For pull-up and push-down transfer, with the neglected effect of viscosity ($Ca < 0.01$) (see Theoretical Analysis in *Materials and Methods*), we will have $\Delta F = b_t(-G_{ts} + \gamma_l\cos\theta_{tl} + \gamma_l)$ for pull-up transfer and $\Delta F = b_t(-G_{ts} + \gamma_l\cos\theta_{sl}^a + \gamma_l)$ for push-down transfer. Besides, for the push-down transfer, a successful transfer requires the transfer energy $(-G_{ts} + \gamma_l\cos\theta_{sl}^a + \gamma_l) < 0$. As a consequence, when the transferred film is pulled out of the liquid bath with the substrate together under the same transfer angle and speed, the transfer energy is $-(-G_{ts} + \gamma_l\cos\theta_{sl}^a + \gamma_l)$, and apparently it is >0, suggesting that the transferred film will keep in good contact with the substrate without detachment. Fig. 3 provides the theoretical phase diagrams on the successful criterion of pull-up and push-down transfer with confirmation of experiments on a wide variety of system materials for soft films, film thickness, transfer substrates, and liquid media. In particular, the experiments show that the success for both transfers is independent of film thickness in a range from hundreds of micrometers to 1 μm, and agree well with theoretical analysis (Fig. 3 and *SI Appendix*, Fig. S7*A*). In addition, compared with the pull-up transfer, because of the dependence on capillary number *Ca* of θ_{sl}^a, the success of push-down transfer will be enhanced by an increased *Ca* (Fig. 3 and *SI Appendix*, Fig. S7*B*). More importantly, taking the capillary number $Ca = 0.01$, the transfer speed can be 3 orders of magnitude higher than conventional transfer methods (*SI Appendix*, Fig. S7*C*) and could be even higher after optimization of systemic parameters such as G_{ts}/γ_l (*SI Appendix*, Fig. S5). Such high transfer speed is further demonstrated in *SI Appendix*, Fig. S7, and its dependence with transfer directions also agrees well with theoretical predictions. We should note that the trapped liquid between substrate and film might exist after both transfers, and the resultant deformation of films due to its subsequent drying out is far less than its elastic strain limit and can be neglected even for the film down to 1 μm in thickness (Theoretical Analysis in *Materials and Methods*). Such negligible deformation is also confirmed with the almost same surface

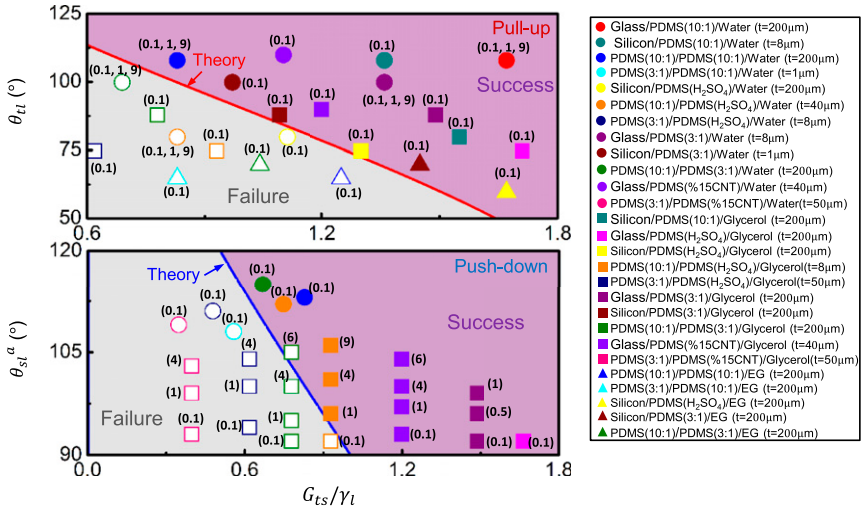

Fig. 3. Criterion for successful capillary transfer of soft films. Theoretical phase diagrams on the successful conditions of capillary transfer, which are confirmed on a wide variety of system materials for receiver substrate, soft film, liquid media, film thickness, and transfer speed. In the theoretical diagram, the red and blue curves represent the theoretical predictions on critical condition of successful transfer for pull-up and push-down directions, respectively. The symbols represent the experimental results, where the open symbol denotes a failure of transfer, the solid symbol denotes a successful transfer; colors and shapes of symbol denote material types of solid substrate/film and liquid environment, respectively. EG represents the ethylene glycol, and the ratio of base polymer to cure agent in PDMS, addition of CNTs to PDMS (wt %), and surface treatment by H_2SO_4 are given in brackets. The transfer speed U is highlighted with the bracket () and the unit is mm/s. For each case of transfer, the experiment was repeated 10 times. The transfer was considered to be successful if the successful rate was larger than 50%, and otherwise it was considered to fail.

topography of the film before transfer and after 24 h of transfer (*SI Appendix*, Fig. S8).

Harnessing Capillary Transfer to Achieve On-Demand Transfer and Assembly of Soft Films. This capillary transfer has many potential applications that enable assembly of film structures with on-demand surface patterns and properties. To illustrate these capabilities, we performed extensive experiments on transfer of conductive composite solid and patterned films. Fig. 4*A* demonstrates a transfer of PDMS/CNT composite film (thickness in 200 μm) onto glass substrate by the pull-up transfer and onto PDMS substrate by push-down transfer at the transfer speed of 1 mm/s ($Ca = 1.4 \times 10^{-5}$). The pull-up transfer yields the top surface (labeled in T) of PDMS/CNT composite film exposed to air for use. By contrast, the push-down transfer yields the bottom surface (labeled in B) of PDMS/CNT (carbon nanotube) composite film exposed to air for use. In parallel, we performed finite-element analysis (FEA) that reproduced the transfer process (see FEA Model in *Materials and Methods* and *SI Appendix*, Figs. S9 and S10). The transfer force at the steady-state transfer process shows good agreement with experiments (*SI Appendix*, Fig. S10). More importantly, the FEA strain analysis (Fig. 4 *A*, *Inset*) shows that the mechanical deformation is not only far smaller than the failure strain of film during both pull-up and push-down transfer processes (elastic limit of film ∼10%, *SI Appendix*, Fig. S9), but will also fully recover with zero strain after successful transfer onto both substrates, suggesting that both transfers will not cause any potential damage during transfer process or leave any residual strain to the film after transfer. To further confirm the negligible mechanical deformation of film after transfer, we measured and compared the electrical resistance of PDMS/CNT composite film as fabricated and after transfer. Remarkable consistence between them is obtained after both transfers (Fig. 4*B*). When the concentration of CNTs in composite films changes, this consistence is maintained. In particular, when the CNT concentration is as high as 25%, it leads to an electrical resistance down to ∼4 $k\Omega$ due to formation of CNTs networks in the film. Such very sensitive microstructures to mechanical deformation remains, as supported by unchanged electrical resistance after transfer onto substrates by either pull-up or push-down transfer, indicating potential applications in transfer of flexible/stretchable electronic devices with very fine microstructures (20). We further compared the surface wettability of as-fabricated and after-transferred films by measuring the contact angle of water droplet on both film surfaces with a series of CNT concentration. The contact angle of PDMS/CNT composite film remains unchanged after transfer in both directions (Fig. 4*C*), independent of CNT concentrations. Although the measured contact angles in both film surfaces are different because of surface roughness that is obtained in the preparation of composite films in an open Petri dish (*SI Appendix*, Fig. S9*B*), they remain unchanged after the capillary transfer onto substrates (Fig. 4*D* and *SI Appendix*, Fig. S11 *A* and *B*). The unaffected electrical function and surface wettability of films also indicates that the mechanical deformation associated with the drying out of possibly trapped water between film and substrate after transfer can be neglected, consistent with theoretical analysis and surface morphology on the characterization of PDMS thin film (*SI Appendix*, Fig. S8). When the smooth and rough surface of composite film is switched on the water surface, this composite film is also successfully transferred onto substrates (*SI Appendix*, Fig. S11*C*). Accordingly, the film surface is also flipped over with rough and smooth surface exposed to air after pull-up and push-down transfer, respectively, and the electrical resistance and surface wettability of the film remain after transfer (*SI Appendix*, Fig. S11 *D–F*). These demonstrations on the same film but an opposite surface side in contact with the substrate indicate that the capillary transfer approach can be well applied to achieve desirable surface functions of films such as Janus films by solely controlling the direction of transfer.

To demonstrate the capability of capillary transfer for films with complex and delicate patterns, three PDMS/CNT composite films with "University of Virginia (UVA)" letters, logo, and kirigami patterns, respectively have been made and successfully transferred to a glass and PDMS substrate from a water surface using both pull-up and push-down methods (Fig. 4*E* and *SI Appendix*, Fig. S12 *A–D*). Besides, FEA results confirm that the maximum strain in the patterned films is much smaller than the elastic limit (>10%) of film materials during the entire transfer

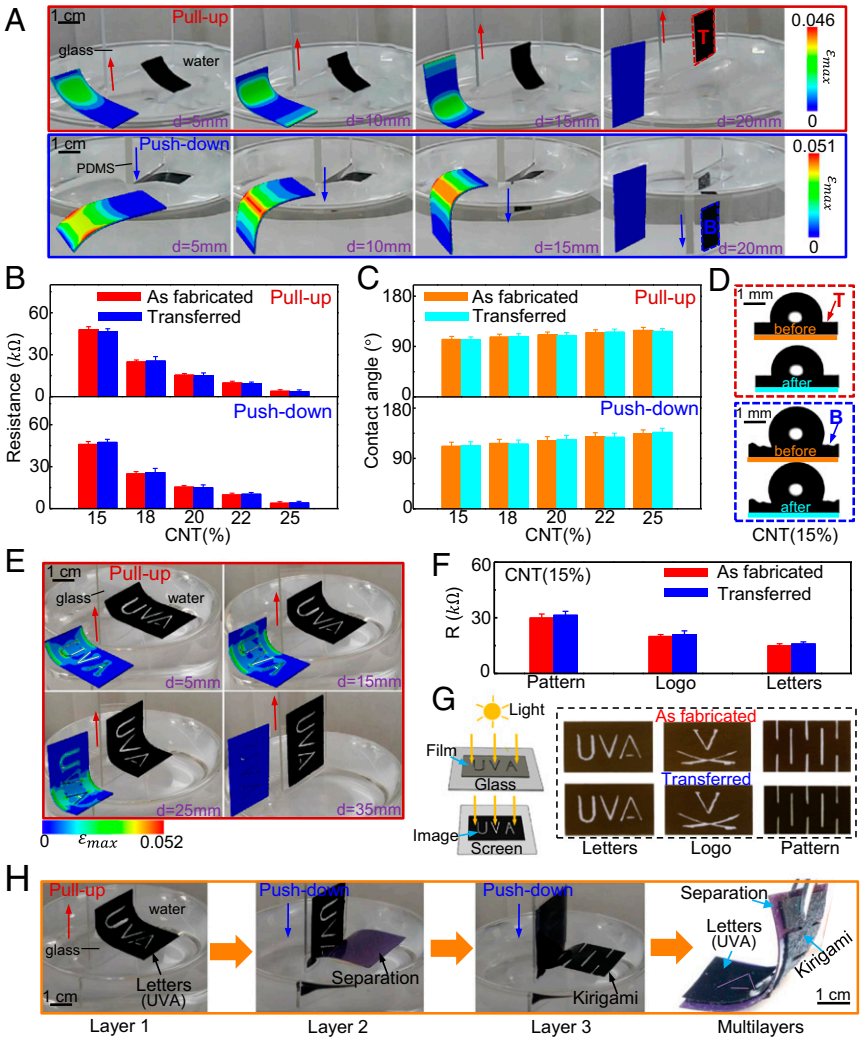

Fig. 4. Demonstrations on the applications of capillary transfer approach. (*A*) Capillary transfer of PDMS/CNT composite film (thickness in 200 μm) from water surface to glass slide by pull-up transfer and to PDMS slide by push-down transfer. The pull-up transfer yields the top surface (marked with the red T) of composite film exposed to air for use. By contrary, the push-down transfer yields the bottom surface (marked with the blue B) of composite film exposed for use. (*Inset*) FEA plane-strain distribution on the film during both transfer processes, which is far smaller than its maximum failure strain (>20%). (*B*) Comparison of measured electrical resistance of PDMS/CNT composite film before and after transfer using both pull-up and push-down transfer. Error bar represents the SD from the mean of three independent measurements. (*C*) Comparison of measured contact angle of water droplet on the top (smooth) surface (via pull-up transfer) and bottom (rough) surface (via push-down transfer) of composite film before and after transfer. Error bar represents the SD from the mean of three independent measurements. (*D*) Experimental images of water droplet on the top (smooth) surface (red T) and bottom (rough) surface (blue B) of PDMS/CNT composite film before (orange line) and after transfer (blue line). (*E*) Experimental and FEA simulation snapshots of the capillary transfer of PDMS/CNT composite film with UVA letters pattern. (*F*) Comparison of measured electrical resistance of composite film with three different patterns before and after transfer. Error bar represents the SD from the mean of three independent measurements. (*G*) Schematic illustration of the optical imaging method (*Left*) and comparison of imaging characteristics of three patterned films before and after pull-up transfer (*Right*). (*H*) Assembly of multilayered soft-film structures by combination of push-down and pull-up capillary transfer. The transfer generates a composite layered structure with two different surface patterns after peeling from the substrate.

processes and the deformation also fully recovers after completion of transfer, indicating a successful transfer and preservation of the complex and delicate patterns and structures onto substrates. The electrical resistance was measured and remains the same before and after transfer (Fig. 4*F* and *SI Appendix*, Fig. S12*E*), which proves that both the pattern and function of the film were not changed by the transfer process. Comparison of imaging characteristics of these three patterned films before and after transfer further confirms that the fidelity of these patterns is precisely maintained (Fig. 4*G* and *SI Appendix*, Fig. S12*F*). The capability of capillary transfer in assembly of multilayered soft-film structures is demonstrated by rationally selecting and combining these two directions of push-down and pull-up transfer (Fig. 4*H*). The PDMS/CNT composite film with UVA pattern was first transferred from water surface to glass slide using the pull-up transfer. Next, a PDMS layer (dyed in purple) was transferred onto the film substrate with the UVA pattern through the push-down transfer. Afterward, the PDMS/CNT composite film with kirigami structure was transferred onto this dyed PDMS layer, generating a composite layered structure with two different surface patterns after peeling from the substrate (Movie S3).

Conclusion

In summary, the capillary transfer technology presented here represents a powerful approach to transfer soft films from surface of liquid onto a solid substrate in a fast and defect-free manner. The fundamental theoretical model and transfer criteria, validated with comprehensive experiments and FEAs, provide a quantitative

guide and optimization for the choice of material systems, operating conditions, and environments for scalable on-demand transfers with high yield. Moreover, the intrinsically moderate capillary transfer force and externally selectable transfer direction offer robust capabilities for achieving deterministic assembly and surface properties of structures with complex layouts and patterns for potentially broad applications in the fabrication of flexible/stretchable electronics, surface-wetting structures, and optical devices. Integration of this technology with other advanced manufacturing technologies associated with material self-assembly, growth, and layout alignment represents promising future topics and would also help create emerging manufacturing technologies that leverage unique fluidity of liquid environments.

Materials and Methods

Materials. In the fabrication of PDMS film, PDMS (Sylgard 184, Dow Corning Corp.) with 10:1 (otherwise stated) of base polymer to cure agent was first mixed and degassed. The mixture was then poured into a Petri dish and placed in 150 °C oven for 1 h to cure. In the fabrication of PDMS/CNT composite film, PDMS with 10:4 base polymer to hexane (n-Hexane, anhydrous, 95%, Sigma-Aldrich) was first mixed and then followed by the addition of multiwalled CNTs (8–15 nm in diameter, 10–15 μm in length, 95%, NanoAmor Inc.). The PDMS-Hexane/CNTs mixture was placed in an ultrasonicator for at least 12 h with 40 kHz to achieve a homogeneous distribution of CNTs. Afterward, the PDMS curing agent was added to cure the mixture at 80 °C for 1 h. In the fabrication of patterned PDMS/CNT film, a mold with desired pattern (letters, logo, and kirigami pattern) was first fabricated using the 3D printer (Objet Connex 500, Stratasys Inc.), and then the printed mold was pressed onto the liquid PDMS/CNT mixture before the cure. After the cure, the mold was removed and the patterned film was left in the Petri dish.

Chemical treatment was conducted to tune the surface wettability of as-fabricated PDMS film by utilizing Piranha solution that introduces OH group at the surface of PDMS film and modifies the wettability (21). Dilution of 50% hydrogen peroxide (Sigma-Aldrich) to 30% with deionized (DI) water was carried out in a beaker, and then followed by the addition of 98% sulfuric acid (Acros Organics) in a volume ratio of 3:1. The as-prepared Piranha solution was then poured on PDMS films in Petri dish and then soaked for 15–30 min depending on the desired wettability. After that, films were rinsed by DI water and finally dried in air.

Characterization of Surface Wettability. In the measurement of static contact angle θ^s_{sl}, a liquid droplet with volume ∼3 μL was first pipetted onto the target surface of solid material. The image of the profile of the liquid droplet was then captured using the goniometer system (Ramé-Hart 200–00). Afterward, the analysis software, DROPimage Standard, was used to process the image to obtain θ^s_{sl}. The measurement of dynamic contact angles between solid substrate and liquid was conducted in tensiometer (Krüss K100) (*SI Appendix*, Fig. S1*A*), detailed below. The substrate was held by the force gauge of the tensiometer and was pushed down into or pulled up out of the liquid bath in depth H with a velocity U. During the push-down process that corresponds to the push-down transfer, the contact angle between substrate and liquid increases from the static contact angle θ^s_{sl}, until approaching an equilibrium contact angle which is the advancing dynamic contact angle θ^a_{sl} (*SI Appendix*, Fig. S1*B*). Simultaneously, the variation of capillary force with the moving displacement of substrate is also recorded, and at the equilibrium steady-state stage, the capillary force is F^a_s. The θ^a_{sl} can be determined via $\cos\theta^a_{sl} = F^a_s/\gamma_l L_p$, where γ_l is the liquid surface tension and L_p is the perimeter of the substrate. By contrast, during the pull-up process that corresponds to the pull-up transfer, the contact angle decreases from the static contact angle θ^s_{sl} to an equilibrium contact angle which corresponds to the receding dynamic contact angle θ^r_{sl} (*SI Appendix*, Fig. S1*C*). The θ^r_{sl} is determined via $\cos\theta^r_{sl} = F^r_s/\gamma_l L_p$, where F^r_s is the equilibrium force during the pull-up process. The force is negative when its direction is downward and is positive when it is upward. In addition, the static contact angle θ^s_{sl} measured from the goniometer system (Ramé-Hart 200–00) can be confirmed from dynamic contact angles via $\cos\theta^s_{sl} = \frac{\cos\theta^a_{sl} + \cos\theta^r_{sl}}{2}$ (22).

Capillary Transfer Experiments. In the capillary transfer experiments, a clean substrate was first submerged in the liquid and was in contact with one end of the desired film to form the contact line (referred to as the transfer front), where the film was placed in the liquid surface with the help of soluble tape and could also be printed directly. Then the substrate was held by the force gauge of the tensiometer (Krüss K100) to be either pulled up out of or pushed down into the liquid bath in the vertical direction ($\alpha = 0°$) with a velocity U. During the motion of substrate, if the transfer was successful, the film would pass across the transfer front, and was gradually transferred onto the moving substrate. If the transfer failed, the film could not pass across the transfer front, and would stay on the liquid surface. During the transfer process, the magnitude of transfer force F and moving displacement d were recorded by the tensiometer. The transfer process was recorded by the high-resolution camera placed near the tensiometer. For each transfer, the experiment was repeated 10 times under the same condition. The transfer was considered to be successful if the successful rate was larger than 50%, and otherwise it failed.

Measurement of Interfacial Adhesion Energy. The peeling test was performed in dry air to measure the adhesion energy G_{ts} at the interface between film and substrate. A layer of film with thickness of 200 μm was first adhered on the target receiver substrate. The as-prepared specimen was firmly attached on the moving stage of the tensiometer with a double-sided tape (Kapton). The film was peeled off from the substrate at one end with 90° peeling angle. During the peeling process, the peeling strength P (applied peeling force per unit of film width) and displacement l were recorded (*SI Appendix*, Fig. S6). The interfacial adhesion energy G_{ts} was calculated via $G_{ts} = P_{ss}$, where the effect of elastic tension deformation of film on the peeling can be neglected with thickness about 200 μm (23), and P_{ss} is the averaged value of the peeling strength at the steady state.

Characterization of PDMS/CNT Composite Films. Uniaxial tensile test was performed to measure the Young's modulus E of film. The test specimen was 100 mm in overall length, 30 mm in overall width, and 1 mm in thickness. The initial linear stage of the tensile stress–strain curves was used to extract the Young's modulus E (*SI Appendix*, Fig. S9*A*). The failure strain was defined where the stress began to drop. In addition, during the curing process of PDMS/CNTs solution, because the bottom side was in contact with the Petri dish but the top side was exposed to air, this manufacturing process led to a rough top surface and a relatively smooth bottom surface of PDMS/CNTs film, as confirmed by the Hiroc RH-8800 3D digital light microscope (*SI Appendix*, Fig. S9*B*). Peeling test was performed to measure the adhesion energy G_{ts} of both top (rough) and bottom (smooth) surfaces of PDMS/CNTs composite film with substrate (*SI Appendix*, Fig. S9*C*), and the measured interfacial adhesion energy is summarized in *SI Appendix*, Fig. S9*D*.

Theoretical Model and Analysis. At the initial state of transfer with the substrate moving velocity U, the essential deformation of the soft film at the transfer front (i.e., contact line among substrate, film, and liquid) (24–27) results from the energy competition among the elastic bending deformation $(E_{bending})$ of the soft film, the elastic elongation (stretching) deformation of the soft film $(E_{elongation})$, and the solid–liquid capillary interaction $(E_{surface})$ can be quantified through the minimization of total energy via $E_t = E_{bending} + E_{elongation} + E_{surface}$, where $E_{bending} = \int_0^{L(1+\varepsilon)} \frac{Bb_t}{24} k^2 ds$ and $E_{surface} = -\gamma_l \cos\theta^d_{sl} b_t \sqrt{\frac{\gamma_l}{\rho g}} \cot\phi/\cos\alpha$; $B = Et^3$ is the bending stiffness of the soft film, E, t, and b_t are the elastic modulus, thickness, and width of the soft film, respectively; ε is the elongation (stretching) strain, k is the local curvature, and L is the length of the soft film; γ_l is the surface tension of liquid, ρ is the liquid density, ϕ is the tangential direction of the bent soft film at the transfer front with respect to the vertical $(-y)$ direction (Fig. 1*A*), and α is the direction of substrate relative to the vertical $(-y)$ direction; θ^d_{sl} is the dynamic contact angle of the substrate to the liquid, and θ_{tl} is the contact angle of the soft film to the liquid. When the soft film begins to be transferred from the liquid surface, it could be stretched by the capillary force (per unit width) $\gamma_l \cos\theta_{tl}$ and/or viscous force (per unit width) $\mu U \frac{L}{H}$, where μ is the liquid viscosity, U is the transfer velocity (i.e., substrate moving velocity), and H is the depth of liquid bath (*SI Appendix*, Fig. S1*A*). The elongation strain of the soft film can be obtained, which is $\varepsilon = \left|\frac{\gamma_l \cos\theta_{tl} + \mu U \frac{L}{H}}{Et}\right|$ and the resultant elastic elongation energy is $E_{elongation} = (Lb_t t)\left(\frac{1}{2}\varepsilon^2 E\right) = \frac{\left(\gamma_l \cos\theta_{tl} + \mu U \frac{L}{H}\right)^2 Lb_t}{2Et}$. Consider the surface tension of water $\gamma_l = 0.072$ N/m, surface wettability of PDMS film θ_{tl}(∼110°), transfer speed U (<700 mm/s, i.e., the capillary number $Ca < 1 \times 10^{-2}$,where the effect of viscosity can be neglected), the water viscosity (∼0.001 Pa s), and the PDMS film with modulus E (∼2 MPa) and thickness t (∼200 μm) used in our experiments, the elongation energy per unit width $E_{elongation}/b_t = \frac{\left(\gamma_l \cos\theta_{tl} + \mu U \frac{L}{H}\right)^2 L}{2Et}$ is $\sim 10^{-7}$ J/m. Besides, consider the capillary length $\sqrt{\frac{\gamma_l}{\rho g}} \approx 3$ mm; the interfacial energy per unit width

$E_{surface}/b_t = -\gamma_l \cos\theta_{sl}^d \sqrt{\frac{\gamma_l}{\rho g}} \cot\phi/\cos\alpha$ is $\sim 10^{-4}$ J/m. Therefore, in comparison with the interfacial energy per unit width, the contribution of elongation energy $E_{elongation}$ can be neglected, and the deformation of the soft film at the transfer front at the initial state of transfer is dominated by the competition between elastic bending deformation ($E_{bending}$) and solid–liquid capillary interaction ($E_{surface}$), where $E_{bending} = \int_0^L \frac{Bb_t}{24} k^2 ds = \int \frac{1}{2}\left(\frac{Bb_t}{12}\right)(y''/(1+y'^2)^{3/2})^2 (1+y'^2)^{1/2} dx$ due to the negligible ε. As a result, the profile of the soft film at the transfer front can be characterized by the geometric analysis with bending deformation via $y = \sqrt{\frac{\gamma_l}{\rho g}} \cot\phi e^{-x\sqrt{\rho g/\gamma_l}}$.

At the steady-state transfer process, the energy principle is further formulated to calculate the magnitude of the transfer force. Consider a small motion distance of substrate Δd, the work done by the transfer force is $\Delta E^F = F_s \Delta d$, where F_s is the magnitude of steady state transfer force. The associated change of the interfacial energy in the pull-up transfer is $\Delta E_{surface} = 2(\gamma_l \cos\theta_{sl}^r) b_s \Delta d + (-G_{ts} + \gamma_l \cos\theta_{tl} + \gamma_l) b_t \Delta d$, where G_{ts} is the adhesion energy between thin film and substrate, θ_{tl} is the contact angle of film to liquid, b_t is the width of film, and b_s is the width of substrate. For the push-down transfer, the associated change of interfacial energy is $\Delta E_{surface} = -2(\gamma_l \cos\theta_{sl}^a) b_s \Delta d + (-G_{ts} + \gamma_l \cos\theta_{sl}^a + \gamma_l) b_t \Delta d$. Because the bending profile of the soft film keeps unchanged during the steady-state transfer, the elastic bending energy remains constant, and the associated variation of the elastic deformation energy $\Delta E_{deformation}$ only results from the elongation (stretching) deformation of the soft film, which is $\Delta E_{deformation} = -\left(\gamma_l \cos\theta_{tl} + \mu U \frac{L}{H}\right)^2 b_t \Delta d / 2Et$. The dissipated energy due to the viscous effect of liquid is $\Delta E_D = \mu U b_t \frac{L}{H} \Delta d$ (28). Therefore, the energy balance at the steady-state transfer of film requires $\Delta E^F = \Delta E_{surface} + \Delta E_D + \Delta E_{deformation}$. Based on the above analysis, the contribution of elastic elongation energy can be neglected in comparison with the interfacial energy, and the energy balance becomes $\Delta E^F = \Delta E_{surface} + \Delta E_D$. As a result, we have the transfer force $F_s = 2b_s\gamma_l \cos\theta_{sl}^r + b_t(-G_{ts} + \gamma_l \cos\theta_{tl} + \gamma_l) + \mu U b_t \frac{L}{H} = 2b_s\gamma_l \cos(((\theta_{sl}^s)^3 - k_\varepsilon \cdot Ca)^{1/3}) + b_t(-G_{ts} + \gamma_l \cos\theta_{tl} + \gamma_l) + \mu U b_t \frac{L}{H}$ for pull-up transfer and $F_s = -2b_s\gamma_l \cos\theta_{sl}^a + b_t(-G_{ts} + \gamma_l \cos\theta_{sl}^a + \gamma_l) + \mu U b_t \frac{L}{H} = (-2b_s\gamma_l + b_t\gamma_l) \cdot \cos(((\theta_{sl}^s)^3 + k_\varepsilon \cdot Ca)^{1/3}) + b_t(-G_{ts} + \gamma_l) + \mu U b_t \frac{L}{H}$ for push-down transfer. At the capillary number $Ca < 1 \times 10^{-2}$, the effect of viscosity of liquid on the steady-state transfer force F_s can be neglected (*SI Appendix*, Fig. S5), and they are simplified to $F_s = 2b_s\gamma_l \cos(((\theta_{sl}^s)^3 - k_\varepsilon \cdot Ca)^{1/3}) + b_t(-G_{ts} + \gamma_l \cos\theta_{tl} + \gamma_l)$ for pull-up transfer and $F_s = (-2b_s\gamma_l + b_t\gamma_l)\cos(((\theta_{sl}^s)^3 + k_\varepsilon \cdot Ca)^{1/3}) + b_t(-G_{ts} + \gamma_l)$ for push-down transfer. Similarly, the force with substrate only during the pull-up and push-down processes can also be obtained, and they are $F_s = 2b_s\gamma_l \cos\theta_{sl}^r$ for pull-up and $F_s = -2b_s\gamma_l \cos\theta_{sl}^a$ for push-down direction. Therefore, the difference of the transfer force, ΔF, between with and without the transfer of film at the steady state of transfer process is $\Delta F = b_t(-G_{ts} + \gamma_l \cos\theta_{tl} + \gamma_l) + b_t\left(\mu U \frac{L}{H}\right)$ for pull-up transfer, and $\Delta F = b_t(-G_{ts} + \gamma_l \cos\theta_{sl}^a + \gamma_l) + b_t\left(\mu U \frac{L}{H}\right)$ for push-down transfer. When the contribution from the viscosity of liquid $b_t\left(\mu U \frac{L}{H}\right)$ is neglected (*SI Appendix*, Fig. S5), $\Delta F = b_t(-G_{ts} + \gamma_l \cos\theta_{tl} + \gamma_l)$ for pull-up transfer, and $\Delta F = b_t(-G_{ts} + \gamma_l \cos\theta_{sl}^a + \gamma_l)$ for push-down transfer. In addition, if liquid is trapped between film and substrate after transfer, the resultant capillary force (per unit area) exerted on the film by its subsequent evaporation could be estimated via $\left|\frac{\gamma_l \cos\theta_{tl}}{t}\right|$, and can be neglected on the film deformation. For example, consider the liquid water, $\gamma_l = 0.072$ N/m, surface wettability of PDMS film θ_{tl}(~110°), and Young's modulus E(~2 MPa) measured in our experiments; the capillary force is ~19 KPa for PDMS film with thickness $t = \sim 1$ μm and ~100 Pa for PDMS film with thickness $t = \sim 200$ μm, which will lead to ~0.9% and ~0.005% strain for PDMS with thickness of $t = \sim 1$ μm, $t = \sim 200$ μm, respectively, far less than the elastic limit (~10%) of PDMS films.

FEA. FEA (ABAQUS/standard package, Dassault Systèmes) was conducted to simulate the capillary transfer process of film. In FEA (*SI Appendix*, Fig. S10*A*), the plane-strain model was employed to simulate the transfer experiments and the film was considered to be elastic and meshed with four-node bilinear plane-strain elements. The elastic modulus (E) was obtained from the tensile experiments described above (*SI Appendix*, Fig. S9). The substrate and liquid surface were modeled as rigid. Convergence of mesh size and number was tested to ensure computational accuracy. The interaction between film and substrate was modeled using a cohesive zone model with parameters obtained from the peeling test (*SI Appendix*, Fig. S9). In the FEA model, a constant velocity was applied to the free end of the substrate exposed to air in an either upward or downward direction to simulate the pull-up or push-down transfer, meanwhile the liquid surface was fixed. The capillary constraint through a cohesive interaction was applied between film and liquid surface to ensure the film always moved along the liquid surface. Distributed forces were applied to the other end of film and substrate opposite to the moving direction to simulate the capillary interactions between film and liquid, and between substrate and liquid, respectively. The resultant force F and displacement d to the substrate in both pull-up and push-down transfer simulations were extracted to compare with those in the experiments. The agreement of F between simulation and experimental results (*SI Appendix*, Fig. S10*B*) validated the FEA model. The maximum deformation strain in the film during the transfer process was also obtained from the simulations (*SI Appendix*, Fig. S10*C*).

Data Availability. All data supporting the conclusions of this research are available within the paper and/or *SI Appendix* and Movies S1–S3.

ACKNOWLEDGMENTS. This work is supported by the University of Virginia, National Science Foundation grant CMMI-1728149, and Virginia Microelectronics Consortium (VMEC) grant.

1. D.-Y. Khang, H. Jiang, Y. Huang, J. A. Rogers, A stretchable form of single-crystal silicon for high-performance electronics on rubber substrates. *Science* **311**, 208–212 (2006).
2. N. K. Mahenderkar *et al*., Epitaxial lift-off of electrodeposited single-crystal gold foils for flexible electronics. *Science* **355**, 1203–1206 (2017).
3. D.-H. Kim *et al*., Epidermal electronics. *Science* **333**, 838–843 (2011).
4. C. Larson *et al*., Highly stretchable electroluminescent skin for optical signaling and tactile sensing. *Science* **351**, 1071–1074 (2016).
5. B. Tian *et al*., Macroporous nanowire nanoelectronic scaffolds for synthetic tissues. *Nat. Mater.* **11**, 986–994 (2012).
6. A. D. Mickle *et al*., A wireless closed-loop system for optogenetic peripheral neuromodulation. *Nature* **565**, 361–365 (2019).
7. H. Jinno *et al*., Stretchable and waterproof elastomer-coated organic photovoltaics for washable electronic textile applications. *Nat. Energy* **2**, 780–785 (2017).
8. J. Zhao *et al*., Air-stable and freestanding lithium alloy/graphene foil as an alternative to lithium metal anodes. *Nat. Nanotechnol.* **12**, 993–999 (2017).
9. W. Wu *et al*., Piezoelectricity of single-atomic-layer MoS2 for energy conversion and piezotronics. *Nature* **514**, 470–474 (2014).
10. M. Li, H. X. Tang, M. L. Roukes, Ultra-sensitive NEMS-based cantilevers for sensing, scanned probe and very high-frequency applications. *Nat. Nanotechnol.* **2**, 114–120 (2007).
11. X. Chen, L. Mahadevan, A. Driks, O. Sahin, Bacillus spores as building blocks for stimuli-responsive materials and nanogenerators. *Nat. Nanotechnol.* **9**, 137–141 (2014).
12. A. Carlson, A. M. Bowen, Y. Huang, R. G. Nuzzo, J. A. Rogers, Transfer printing techniques for materials assembly and micro/nanodevice fabrication. *Adv. Mater.* **24**, 5284–5318 (2012).
13. J.-K. Chang *et al*., Materials and processing approaches for foundry-compatible transient electronics. *Proc. Natl. Acad. Sci. U.S.A.* **114**, E5522–E5529 (2017).
14. A. Pirkle *et al*., The effect of chemical residues on the physical and electrical properties of chemical vapor deposited graphene transferred to SiO2. *Appl. Phys. Lett.* **99**, 122108 (2011).
15. J. W. Suk *et al*., Transfer of CVD-grown monolayer graphene onto arbitrary substrates. *ACS Nano* **5**, 6916–6924 (2011).
16. I. Jeon *et al*., Janus graphene: Scalable self-assembly and solution-phase orthogonal functionalization. *Adv. Mater.* **31**, e1900438 (2019).
17. P. Xiao *et al*., Hydrophilic/hydrophobic interphase-mediated bubble-like stretchable Janus Ultrathin Films toward self-adaptive and pneumatic multifunctional electronics. *ACS Nano* **13**, 4368–4378 (2019).
18. J. Yan *et al*., Bacterial biofilm material properties enable removal and transfer by capillary peeling. *Adv. Mater.* **30**, e1804153 (2018).
19. R. L. Hoffman, A study of the advancing interface. I. Interface shape in liquid—Gas systems. *J. Colloid Interface Sci.* **50**, 228–241 (1975).
20. J. Park *et al*., Tactile-direction-sensitive and stretchable electronic skins based on human-skin-inspired interlocked microstructures. *ACS Nano* **8**, 12020–12029 (2014).
21. K.-S. Koh, J. Chin, J. Chia, C.-L. Chiang, Quantitative studies on PDMS-PDMS interface bonding with piranha solution and its swelling effect. *Micromachines (Basel)* **3**, 427–441 (2012).
22. M. Miyama, Y. Yang, T. Yasuda, T. Okuno, H. K. Yasuda, Static and dynamic contact angles of water on polymeric surfaces. *Langmuir* **13**, 5494–5503 (1997).
23. K. Kendall, Thin-film peeling-the elastic term. *J. Phys. D Appl. Phys.* **8**, 1449–1452 (1975).
24. R. Masurel, M. Roché, L. Limat, I. Ionescu, J. Dervaux, Elastocapillary ridge as a non-integer disclination. *Phys. Rev. Lett.* **122**, 248004 (2019).
25. M. Zhao *et al*., Geometrical control of dissipation during the spreading of liquids on soft solids. *Proc. Natl. Acad. Sci. U.S.A.* **115**, 1748–1753 (2018).
26. S. Karpitschka *et al*., Droplets move over viscoelastic substrates by surfing a ridge. *Nat. Commun.* **6**, 7891 (2015).
27. E. R. Jerison, Y. Xu, L. A. Wilen, E. R. Dufresne, Deformation of an elastic substrate by a three-phase contact line. *Phys. Rev. Lett.* **106**, 186103 (2011).
28. S. Khodaparast, F. Boulogne, C. Poulard, H. A. Stone, Water-based peeling of thin hydrophobic films. *Phys. Rev. Lett.* **119**, 154502 (2017).